Partial Oxidation of *n*-Pentane over Vanadium Phosphorus Oxide supported on Hydroxyapatites

Sooboo Singh

School of Chemistry and Physics, University of KwaZulu-Natal, Durban, 4000, South Africa.
E-mail: singhso@ukzn.ac.za

Received 14 August 2015, revised 13 November 2015, accepted 20 November 2015.

ABSTRACT

The selective oxidation of *n*-pentane to value-added products, maleic anhydride or phthallic anhydride by vanadium phosphorus oxide loaded on hydroxyapatites as catalysts and oxygen as oxidant was investigated. Hydroxyapatite (HAp) and cobalt-hydroxyapatite (Co-HAp) were prepared by the co-precipitation method and VPO with varying weight percentages (2.5–15.0 %) were loaded on the hydroxyapatite supports by the wet impregnation technique. The catalyst materials were characterized by surface area measurements, elemental analysis, powder X-ray diffraction (XRD), infrared spectroscopy (IR) and temperature-programmed reduction (TPR). VPO is present in two phases, *viz*. $(VO)_2P_2O_7$ and $VOPO_4$. With increase in the VPO loading on the hydroxyapatites, the $(VO)_2P_2O_7$ phase also increased. From catalytic results, a conversion of 75 % of *n*-pentane and selectivity towards maleic anhydride, about 50 % and phthalic anhydride, about 25 %, were consistently achieved with loadings of 5.0 and 7.5 wt. % VPO at 360 °C for GHSVs of 1900 and 2300 h^{-1}. Under optimum conditions, product yields of up to 40 % maleic anhydride and 20 % phthalic anhydride were obtained. It is proposed that the products formed through the diene intermediate.

KEYWORDS

Selective oxidation, *n*-pentane, vanadium phosphorus oxide, hydroxyapatite, maleic anhydride, phthalic anhydride.

1. Introduction

Maleic anhydride (MA) and phthalic anhydride (PA) are precursors used in the manufacture of synthetic fibres, plastics, paints and adhesives[1]. The selective and controlled oxidation of hydrocarbons using heterogeneous catalysts to produce these compounds, occupy an important place in the chemical industry[2,3]. Vanadium phosphorus oxide (VPO) was found to be efficient in converting *n*-pentane to maleic anhydride and phthalic anhydride[4,5]. This catalytic reaction is promoted by the existence of both the vanadyl pyrophosphate (VPP) as well as of $VOPO_4$ phases in VPO[5,6]. Supported VPO catalysts showed an enhancement in the selectivity towards maleic anhydride and phthalic anhydride. Xiao *et al.*[7] used fumed SiO_2-supported VPO catalysts, prepared by deposition-precipitation, for *n*-butane activation. A conversion of 33–40 % of *n*-butane and maleic anhydride selectivity of 65–87 mol % were obtained over the temperatures tested. In another study, Nie *et al.*[8] compared the efficiency of VPO supported on Al-MCM-41 with a large-pore silica-supported VPO catalyst in the activation of *n*-butane. The VPO supported on Al-MCM-41 showed an increase in maleic anhydride (MA) selectivity with a slight decrease in *n*-butane conversion, attributed to the interaction between the VPO component and the Al-MCM-41 support. Recently, VPO supported on alumina was used for propane ammoxidation and was hyped as a potentially interesting catalytic system for the industrial synthesis of acrylonitrile [9]. Michalakos *et al.*[10] studied the variation in the selectivity for the selective oxidation *n*-pentane on vanadium oxide supported on Al_2O_3 and SiO_2. The loadings for the Al_2O_3 samples were 8.2 and 23.4 wt. % V_2O_5 and for the SiO2 samples, 1.0 and 10.0 wt. % V_2O_5. The Al_2O_3-based catalysts were more active than the supported SiO_2 catalysts, but for catalysts of the same support, the activity per mole depended slightly on the loading. At low pentane conversions, the 1 wt. % V_2O_5/SiO_2 produced pentenes and 1,4-pentadiene, whereas the 10 wt. % V_2O_5/SiO_2 produced mainly carbon oxides. The Al_2O_3-based catalysts produced dehydrogenated products. Here, MA was produced with a selectivity of about 80 % at low conversion on the 23.4 wt. % V_2O_5 loaded catalyst, but was a minor product on 8.2 wt. % loaded catalyst. Small amounts of PA were observed on the Al_2O_3-based catalysts, and none was observed on the supported SiO_2 catalysts. This study was corroborated by a separate study conducted by Klose *et al.*[11].

Activation of hydrocarbons depend, to a large extent, on the acid-base properties of the material or on the isolated cations capable of activating C-H bonds[12,13]. Hydroxyapatites (HAp) are bi-functional materials containing acidic and basic sites in the crystal lattice. HAps are useful as materials in bioceramics, adsorbents, catalysts and catalyst support materials. Its hexagonal structure is made up from columns of calcium ions and oxygen atoms which are located parallel to its axis[14–16]. Three oxygen atoms from each PO_4 tetrahedron are shared by one column and the fourth oxygen atom is attached to the neighbouring column. The lattice of HAp is structured to allow substitution of the calcium ions with other cations by ion exchange and ion adsorption or a combination of these methods to improve its catalytic performance[15,17–19]. Co-HAp offers high stability and the OH group within the phosphate framework leads to the formation of active oxygen species which are essential for ODH reactions[14,20,21]. In another study using Co-HAp as the catalyst, Opre *et al.*[22] showed excellent results for the epoxidation of styrene with in dimethylformamide. Hydroxyapatites are efficient as supports, in particular its basic properties are useful for the Knoevenagel reaction in heterogenous media without solvent[23], the water gas shift reaction with gold and ruthenium as the active components[24] and the partial oxidation of methane over nickel-added strontium phosphate incorporating strontium

ISSN 0379-4350 Online / ©2016 South African Chemical Institute / http://saci.co.za/journal
DOI: http://dx.doi.org/10.17159/0379-4350/2015/v69a1

hydroxyapatite[25]. In our previous study[26], we reported the activation of *n*-pentane using V_2O_5 supported on hydroxyapatite as catalysts. V_2O_5 showed excellent redox capabilities. Selectivity towards the anhydrides (MA 40 % and PA 25 %) was obtained with the 5.0 wt. % V_2O_5 at 360 °C at a conversion of about 60 %. At higher weight loadings, although the conversion increased, the selectivity towards the desired products decreased.

In this paper, we report the preparation and characterization of VPO supported on calcium and cobalt hydroxyapatites and the effect of the VPO loading and support interaction, together with different phases present on the catalyst, in the partial oxidation of *n*-pentane.

2. Experimental

2.1. Preparation of Catalysts

The catalytic materials were prepared using methods published previously, with modifications[26,27]. Concentrated ammonia (BDH, Poole, England) was added to a 60 mL solution of $Ca(NO_3)_2{\cdot}4H_2O$ (6.67×10^{-2} mol) (Merck KGa, Darmstadt, Germany) to increase its pH to 11. The calcium solution was subsequently diluted to twice its volume with distilled water. A 100 mL solution of $(NH_4)_2HPO_4$ (4.00×10^{-2} mol) (Merck KGa, Darmstadt, Germany) was also adjusted to pH 11 using ammonia, diluted to 160 mL. The phosphate solution was added drop-wise to the calcium solution over a period of 30 min with continuous stirring at room temperature. A white, gelatinous precipitate that formed was boiled for 10 min with stirring. Thereafter, the precipitate was filtered under vacuum and washed thoroughly with deionised water. The solid was left to dry overnight in an oven set at 100 °C, followed by calcination under the flow of air at 500 °C. In the preparation of the cobalt hydroxyapatite, $Co(NO_3)_2{\cdot}6H_2O$ (Merck KGa, Darmstadt, Germany) was used. The method of preparation of VPO has been extensively reported in literature[3,6,8,9,28]. In a modified method for preparing VPO, a mixture containing V_2O_5 (5.00 g) (BDH, Poole, England) and H_3PO_4 (30 mL, 85 wt. %) (BDH, Poole, England) was added to 100 mL of deionized water and refluxed for 24 h. A yellow solid that formed was filtered, washed thoroughly with deionised water, followed by acetone (BDH, Poole, England) and air-dried in an oven at 110 °C. The resulting solid was then refluxed with isobutanol (50 mL) (Merck KGa, Darmstadt, Germany) for 20 h. The solid was filtered, dried in an oven set at 110 °C for 16 h and calcined through flowing nitrogen in a furnace set at 500 °C. Finally, in the preparation of the supported catalysts, weight percentages of 2.5, 5.0, 7.5, 10.0 and 15.0 VPO were loaded on the HAp and Co-HAp supports by wet-impregnation[29,30].

2.2. Characterization of Catalysts

The surface area of the catalysts was determined by the BET method[30]. Catalysts were pretreated by degassing under N_2 flow overnight at 250 °C using a Micrometrics Flow Prep 060 (Micrometrics, USA). The degassed samples were analyzed in the Micrometrics Gemini 2360 (Micrometrics, USA), fully automatic, multi-point BET surface area analyzer under liquid N_2. The diffraction patterns of the catalysts were recorded in the 2θ range of 2–80 ° using a Phillips PW 1830 X-ray diffractometer system, equipped with Co K_α radiation ($\lambda = 1.7889$). The experimental conditions corresponded to the step size of 0.040 ° (2θ) (number of steps = 1951), and a dwell time of 1 s. The concentrations of Ca, Co, V and P in the catalysts were measured in aqueous HNO_3 by inductively coupled plasma (ICP) using a Perkin Elmer Optical Emission Spectrometer Optima 5300 DV instrument. Standards, 500 ppm Ca, Co, V and P, were purchased from Fluka. FT-IR spectra of the samples were recorded with a Nicolet Impact 420 spectrophotometer in the mid IR (400–4000 cm^{-1}) region using the KBr disc technique (0.5 % dilution). TPR investigations were carried out with a custom made reactor system connected to a thermal conductivity unit. Hydrogen (5 %) in argon was used for the analysis. For heating, a calibrated furnace was used and a temperature control unit monitored the temperature to within 2 °C. The average vanadium oxidation state was determined by means of a redox titration[28,29].

2.3. Measurement of Catalytic Reactions

Catalytic testing was carried out using a continuous, fixed bed tubular stainless steel reactor (i.d. = 10 mm, l = 300 mm) in down flow mode. The organic feedstock, *n*-pentane (Saarchem, South Africa) was injected into the reactor lines by means of a high precision isocratic pump (LabAlliance Series II) and vapourized on-line. The vapour was carried by the oxidant, an oxygen-helium mixture (20 % O_2, balance He) (Afrox, BOC Special Products). Preliminary testing of VPO and the support materials, HAp and Co-HAp were initially conducted. After these preliminary runs, the VPO-supported catalysts were tested. In all testing, the catalyst bed (2 mL) was located at the centre of the reactor, with carborundum (24 grit, Promark Chemicals, South Africa) filling the spaces on either side of the bed and ends plugged with glass wool. The reactor was heated in an electric furnace with K-type thermocouples monitoring the temperature of the furnace and the catalyst bed. The product stream was analysed by Gas Chromatograph (Varian Star 3400) equipped with a FID module and GC-MS (Finnigan MAT GCQ) using capillary columns (J&W HP5-MS, 250 μm diameter). The carbon oxides and light organic compounds were intermittently monitored by a TCD Gas Chromatograph (Buck Scientific, SRI Instruments, USA) using a packed column (6 silica gel/6 molecular sieve). Water was quantified using a Karl Fischer titrator.

3. Results and Discussion

3.1. Catalyst Characterization

The surface areas and the elemental composition of all the catalysts used in the present studies are displayed in Table 1. The BET surface area of HAp of 48 $m^2\ g^{-1}$ agrees with that reported in literature[24]. There is a decrease in the surface area of the materials from 40 to 15 $m^2\ g^{-1}$ with the increase in VPO loading. It is possible that the narrow pores of the support are filled with the active component making it inaccessible to nitrogen molecules, leading to a decrease in the surface area. The total metal content was also determined for each catalyst to investigate its impact on the activity and selectivity of the catalysts. From elemental analysis, the Ca/P ratio for HAp is 1.67 (Table 1) which indicates that stoichiometric hydroxyapatite was prepared. As the loading of VPO on the supports increased, the M/P (M = Ca and Co) ratios decreased due to the contribution of phosphorus from the hydroxyapatite and VPO.

The XRD patterns of HAp (Fig. 1) confirm that the phases belong to stoichiometric hydroxyapatite with the formula, $Ca_{10}(PO_4)_6(OH)_2$ and they match well with the phases reported by Parhi *et al.*[32]. The patterns for supported catalysts showed the presence of $(VO)_2P_2O_7$ (●) peaks at 2θ angles of 18.6 °, 23.1 °, 28.5 °, 29.9 °, 33.7 ° and 36.9 ° whereas a mixture of the $VOHPO_4{\cdot}½\ H_2O$ and $VOPO_4{\cdot}2\ H_2O$ (◆) phases displayed peaks at 2θ angles of 13.2 °, 20.3 °, 21.6 °, 28.9 °, 29.9 °, 41.1 °, 46.3 °, 59.5 ° and 63.8 °. These agreed with patterns reported in literature[33]. For the Co-HAp and Co-HAp-supported catalysts (Fig. 2), the phases confirms the presence of hydroxyapatite although it was found to be

Table 1 BET surface areas and bulk composition of the catalysts determined by ICP-OES for various VPO/HAp and VPO/Co-HAp catalysts.

Catalyst	BET surface area/$m^2\ g^{-1}$		Ca/P [b]	(V + Ca)/P [b]	V/Ca [c]
	Fresh [a]	Spent [a]			
HAp	48	46	1.67	–	–
2.5VPO/HAp	40	39	1.43	1.74	0.217
5VPO/HAp	31	30	1.37	1.70	0.238
7.5VPO/HAp	26	26	1.35	1.69	0.253
10VPO/HAp	21	20	1.33	1.69	0.270
15VPO/HAp	15	13	1.33	1.67	0.285
			Co/P [b]	(V + Co)/P [b]	V/Co [c]
Co-HAp	35	33	1.82	–	–
2.5VPO/Co-HAp	30	28	1.58	1.86	0.178
5VPO/Co-HAp	28	26	1.43	1.73	0.207
7.5VPO/Co-HAp	25	24	1.24	1.56	0.250
10VPO/Co-HAp	19	17	1.18	1.52	0.289
15VPO/Co-HAp	17	14	1.13	1.49	0.314

[a] Obtained in duplicate with a standard deviation of ±1.00.
[b] From ICP (obtained in triplicate with a standard deviation of ±0.02).
[c] From ICP (obtained in triplicate with a standard deviation of ±0.005).

non-stoichiometric. This was also confirmed by the Co/P ratio obtained through ICP-OES which was 1.82 instead of 1.67. The average vanadium number for the catalysts ranged from 4.11–4.46, confirming the presence of the $(VO)_2P_2O_7$ phase.

Fig. 3A and Fig. 3B displays the infrared spectra of HAp, Co-HAp and the supported catalysts. The formation of the hydroxyapatite structure is confirmed.

The signal at 3500 cm^{-1} is the result of the stretching vibration of the OH^- ions at the lattice sites of the HAp crystals[27]. This signal was absent in the spectra of supported samples. A very broad absorption band was evident at 3400 cm^{-1} which suggests the presence of surface water molecules. Bands observed at 1380 cm^{-1} together with the signal at 1600 cm^{-1} are attributed to CO_3[2–15,16,26,33]. Other typical bands were observed at 1090 cm^{-1} and 1040 cm^{-1} due to (ν_{as} (P-O)) and 960 cm^{-1} (ν_s (P-O)). For the supported catalysts, there were additional peaks due to the stretching modes of pyrophosphate, $P_2O_7^{4-}$ (1160, 1120, 755 cm^{-1}).

From TPR analysis, HAp and Co-HAp were not reduced at the temperatures employed[34], whereas for the supported VPO catalysts, reduction occurs in the 500 °C–800 °C range[6]. The TPR profiles for the 5VPO/HAp and 5VPO/Co-HAp, Fig. 4a and Fig. 4b respectively, shows a main peak around 550 °C, attributed to the removal of lattice oxygen related to V^{4+} species in the $(VO)_2P_2O_7$ phase[35].

The shoulders at 550 and 625 °C for the 15VPO/HAp and 15VPO/Co-HAp, respectively, is attributed to the removal of lattice oxygen related to V^{5+} species (Fig. 4c, d)[35–37]. Small peaks were observed between 400 and 450 °C for both the catalysts due

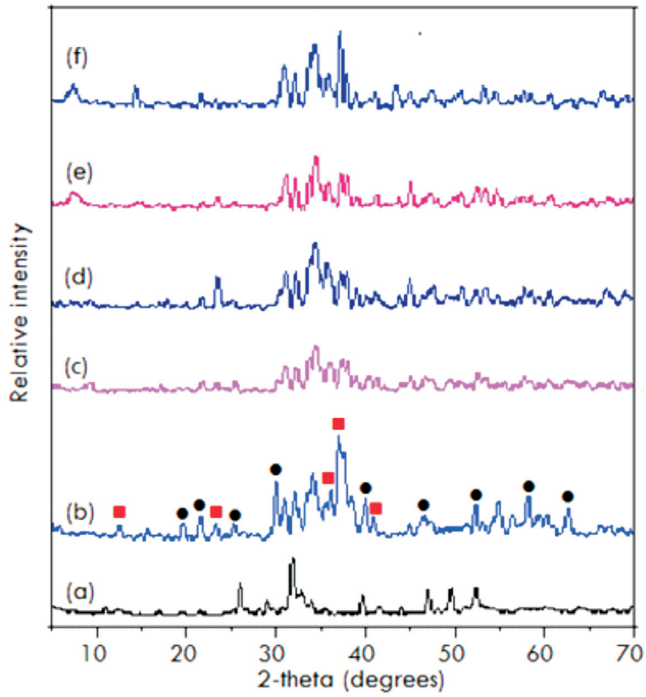

Figure 1 XRD patterns of (a) HAp and (b) 2.5, (c) 5.0, (d) 7.5, (e) 10.0, (f) 15.0 wt. % VPO on HAp; $(VO)_2P_2O_7$ (●) and $VOPO_4{\cdot}x\ H_2O$ (■).

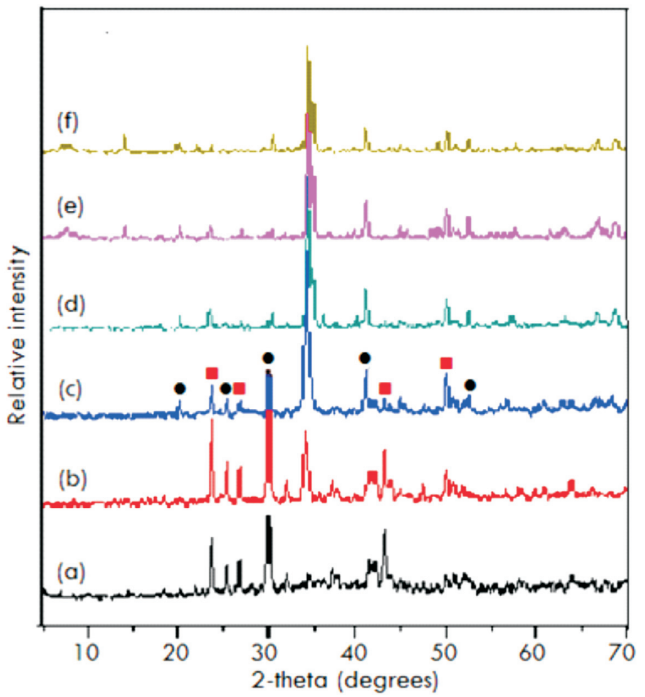

Figure 2 XRD patterns of (a) Co-HAp and (b) 2.5, (c) 5.0, (d) 7.5, (e) 10.0 , (f) 15.0 wt. % VPO on Co-HAp; $(VO)_2P_2O_7$ (●) and $VOPO_4{\cdot}x\ H_2O$ (■).

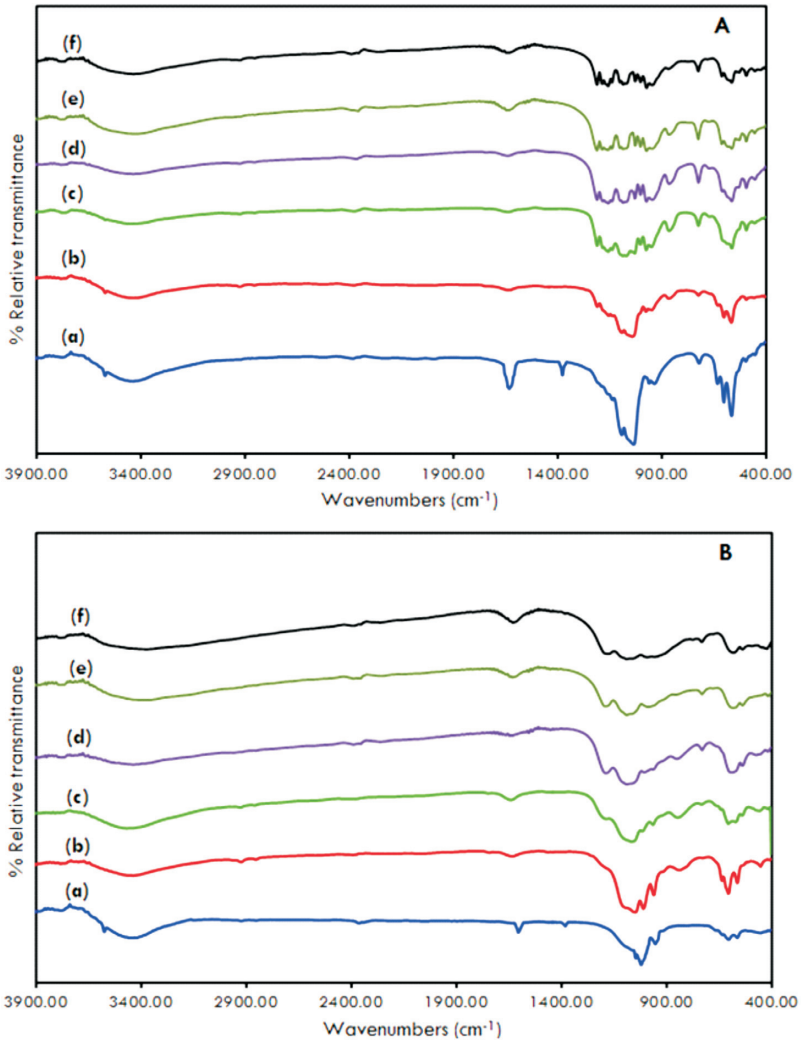

Figure 3 Infrared spectra of (a) HAp and (b) 2.5, (c) 5.0, (d) 7.5, (e) 10.0, (f) 15.0 wt % VPO on (**A**) HAp and (**B**) Co-HAp.

to the agglomerated VPO or the small amounts of vanadium orthophosphates present on the surface of the catalysts[38]. The reducibility of the VPO phase, in general, increased with an increase in vanadium loading.

3.2. Catalytic Testing

The partial oxidation of *n*-pentane in the gas phase with molecular oxygen was investigated with different loadings of VPO supported on HAp and Co-HAp using a fixed-bed continuous flow stainless steel reactor. The experiments were carried out at different flow rates and over a temperature range of 240–440 °C. Steady state for the reactions was established after 3 h. Blank runs conducted using the reactor filled with carborundum (24 grit) showed about 1.00–2.50 % conversion of *n*-pentane producing mainly, carbon oxides (carbon monoxide and carbon dioxide). The activity increased to between 4.5 and 10.0 % with the use of hydroxyapatites as catalysts. The product stream consisted of lower hydrocarbons, oxygenated compounds, carbon oxides and very small amounts 1,3-pentadiene, furan and furfural. For the supported catalysts, the major products obtained were phthalic anhydride, maleic anhydride, carbon oxides, benzoic acid, furan, 2H-pyran-2-one and acetic acid. The minor compounds which are termed as 'others' included the C_2-C_4 hydrocarbons, ethyl acetate, propanoic acid, 1,3-pentadiene, 2-cyclopenten-1-one, furfural, furaldehyde and 1,4-dioxane-2,3-diol.

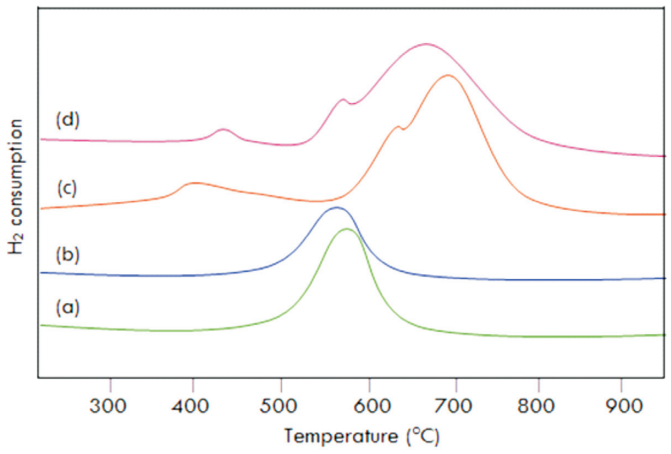

Figure 4 Temperature programmed reduction profiles of (a) 5VPO/HAp, (b) 5VPO/Co-HAp, (c) 15VPO/HAp and (d) 15VPO/Co-HAp catalysts.

To investigate the effect of GHSV, the 5VPO/HAp and 5VPO/Co-HAp catalysts were screened over the GHSV ranges of 1500 to 2700 h^{-1} at a temperature of 360 °C. Fig. 5 shows the typical profiles of the *n*-pentane conversion and the selectivity towards maleic anhydride and phthalic anhydride as a function of GHSVs. With increase in GHSV the conversion of *n*-pentane decreased due to the lower residence time of *n*-pentane on the catalyst. The best results were obtained at GHSVs of 1900 h^{-1} and 2300 h^{-1}. Above GHSV values of 2300 h^{-1}, the selectivity towards

phthalic anhydride (PA) and maleic anhydride (MA) decreased with selectivity towards carbon oxides increasing significantly. All catalytic runs were done in triplicate with an error of ±2.00 % and carbon balances ranged from 97 to 102 %.

Reactions in this study were carried out at six temperatures ranging from 240 to 440 °C. All catalysts showed an increase in activity with an increase in reaction temperature. Fig. 6a shows the conversion and selectivity as a function of temperature using the 5.0 wt. % VPO catalysts.

For the VPO/HAp catalyst, the conversion of the substrate increased gradually from 30 % at 240 °C to 69 % at 360 °C. There was no significant increase in the conversion above 360 °C. For the VPO/Co-HAp, although the maximum conversion was obtained at 440 °C, the selectivity to maleic anhydride was at its highest (50 %) at 360 °C for a conversion of 64 %. At higher temperatures, the MA and PA production decreased while the formation of carbon monoxide and carbon dioxide increased. Similar patterns of activity and selectivity were displayed by the 7.5 wt. % VPO-supported catalysts at the same flow rate (Fig. 6b). The effect of reaction temperature on *n*-pentane conversion and the product yields over 'non-equilibrated' and 'equilibrated' VPO catalysts showed that the yield in maleic anhydride increases from 280 to 400 °C, leveling at 370 °C, while the phthalic anhydride yield reaches a maximum at 350 °C and then decreases with an increase in the formation of the carbon oxides[39]. Similar trends were observed by Bignardi *et al.*[40], who showed that the selectivity towards maleic anhydride increased with an increase in the reaction temperature but the selectivity towards phthalic anhydride decreased.

Weight percentages of 2.5, 5.0, 7.5, 10.0 and 15.0 % VPO were loaded on the hydroxyapatite supports. A marginal difference in the activity of HAp and Co-HAp as supports for VPO was observed. This is due to the easily reducible nature of VPO/Co-Hap which is evident in the TPR profile. The best performing catalysts were the 5.0 and 7.5 wt. % VPO loadings for a reaction temperature of 360 °C with GHSV values of 1900 and 2300 h^{-1} as reflected in Fig. 7. For the 5VPO/HAp catalyst, selectivity towards maleic anhydride and phthalic anhydride was 49 and 11 %, respectively, for a 68 % conversion of *n*-pentane with the GHSV fixed at 1900 h^{-1}. The selectivity towards these products improved marginally when the GHSV was set at 2300 h^{-1}. Using the 5VPO/Co-HAp catalyst, the selectivity towards maleic anhydride and phthalic anhydride was 52 and 22 %, respectively, for a 64 % conversion of *n*-pentane. However, there was a

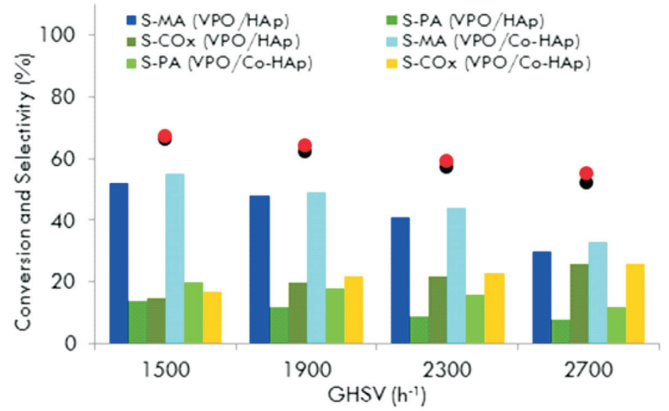

Figure 5 Conversion and selectivity as a function of GHSV over the 5.0 wt. % VPO catalyst at 360 °C (All data points in triplicate with an error of ±2.00 %).

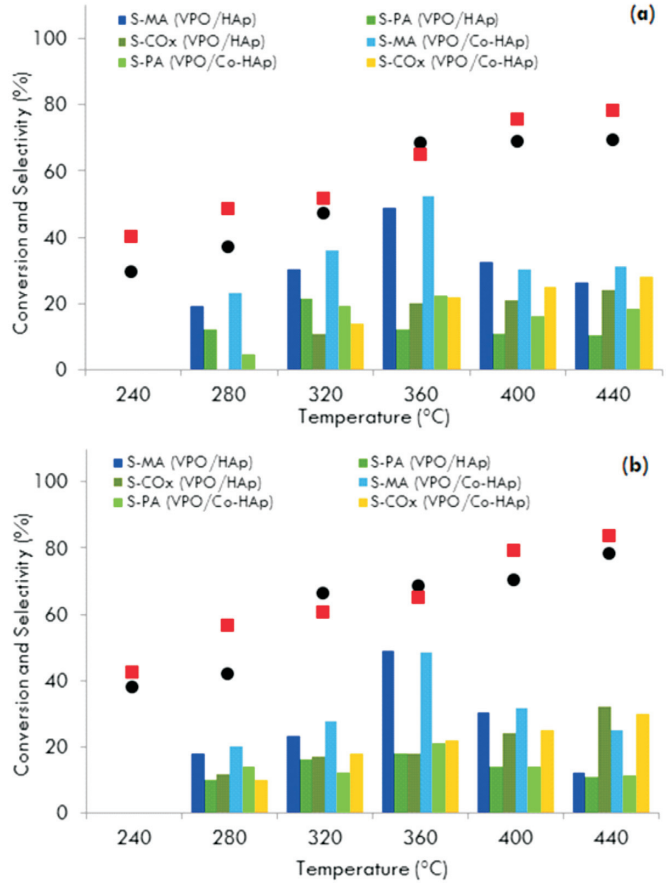

Figure 6 Conversion and selectivity as function of temperature over the (**a**) 5.0 and (**b**) 7.5 wt. % catalysts; GHSV = 1900 h^{-1}. (All data points in triplicate with an error of ±2.00 %.).

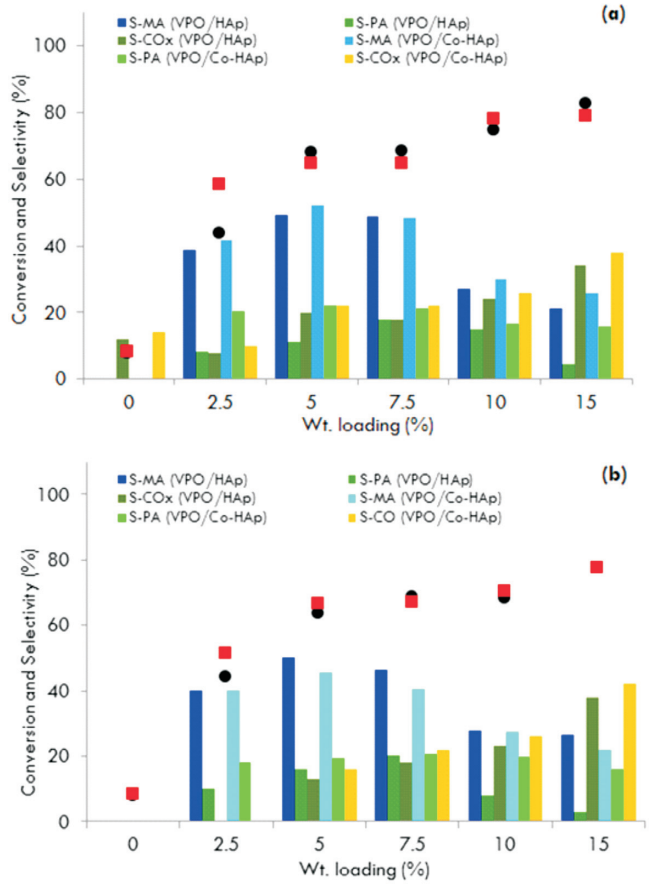

Figure 7 Conversion and selectivity as a function of VPO loading at 360 °C; GHSV fixed at (**a**) 1900 h^{-1} and (**b**) 2300 h^{-1}. (All data points in triplicate with an error of ±2.00 %.).

slight decrease in the amounts of maleic anhydride and phthalic anhydride when the GHSV was set at 2300 h^{-1}. There was a significant increase in the activity in terms of conversion of *n*-pentane, but a slight decrease in the formation of maleic anhydride and phthalic anhydride with an increase in the VPO loadings on both the supports. This could be attributed to the non-crystalline nature of the catalyst surface due to clustering of the VPO at higher loadings leading to a decrease in V^{+4} sites. Lower yields of maleic anhydride and phthalic anhydide at higher VPO loadings could also be the result of an increase in the total metal content of the catalyst.

At higher VPO loadings, both the catalysts showed the similar pattern in conversion but different patterns in the selectivity. The similar trend in conversion is due to a similar reduction pattern observed in TPR and the difference in the selectivity is related to the Ca/P and Co/P ratios. Also, phosphorus stabilizes the active +4 valence state of vanadium and influences its oxidation properties[3,5,9]. In the supported VPO catalysts, phosphorus is present in the hydroxyapatite and VPO and there is a substantial increase in the amount of phosphorus at higher VPO loadings.

3.3. Proposed Mechanistic Pathway for the Formation of 1,3-Pentadiene

In the mechanism for the formation of MA and PA from *n*-pentane, the dimeric active site in VPP undergoes possibly a one- or two-electron oxidation by the adsorbed dioxygen or atomic oxygen and is attached to the hydroxyapatite support through the formation of a metal-oxygen bond. The presence of 1,3-pentadiene in the product stream together with ratios of the anhydride production suggests that both MA and PA forms via a common intermediate, a diene.

The initial activation of *n*-pentane occurs by hydrogen abstraction from a methylene group forming a hydroperoxy moiety bound to the surface and an alkoxy group on the adjacent vanadyl group. The hydroperoxy group then abstracts a hydrogen atom from α-position in the alkoxy group to produce the surface bound species, releasing a water molecule. The surface bound moiety gets protonated forming a carbocation species and the catalyst is regenerated. The loss of a proton and water molecule leads to the formation of pentadiene (Scheme 1). The pentadiene is oxidized to MA, or transformed to cyclopentadiene

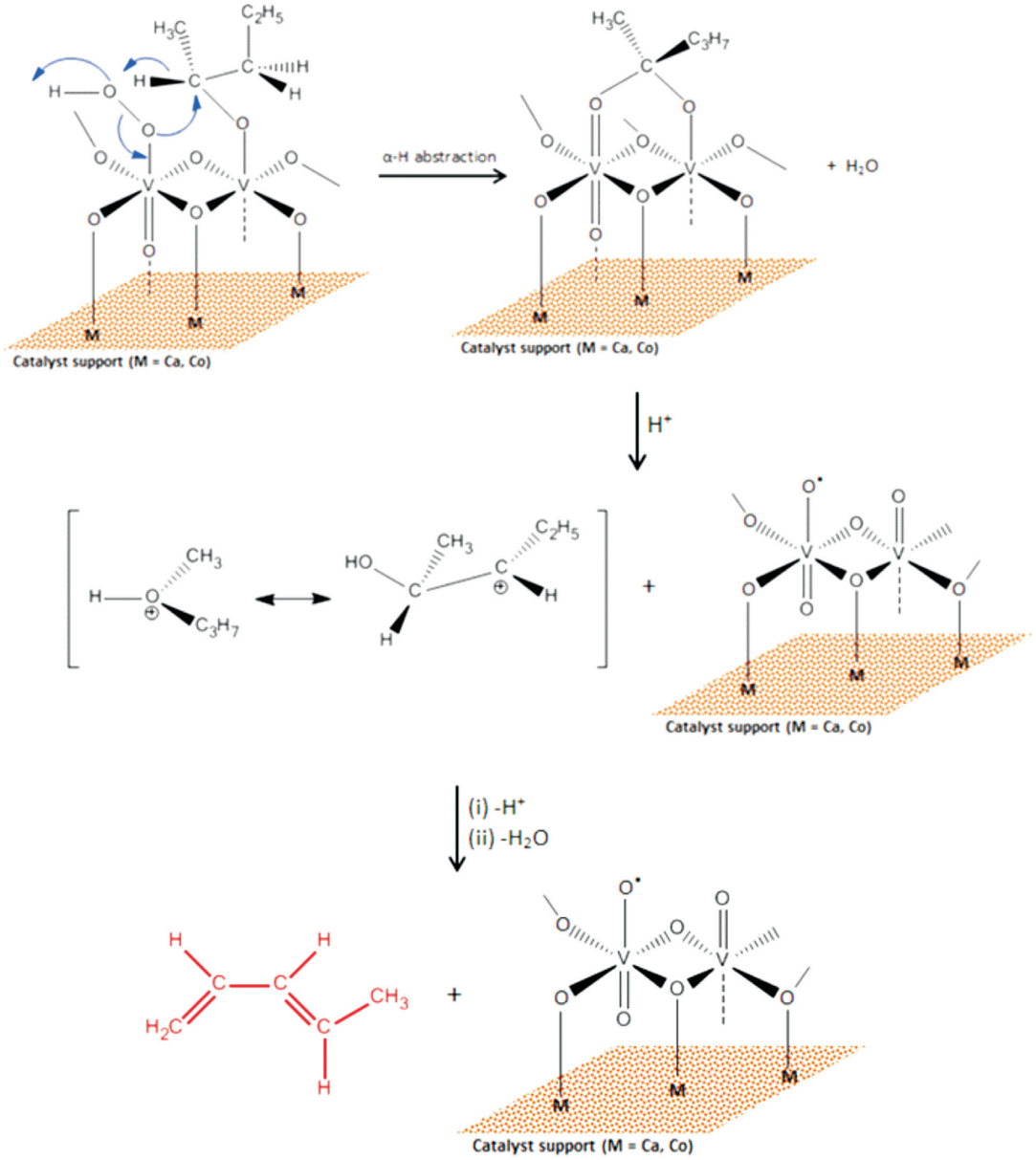

Scheme 1
Mechanism for the formation of the carbocation and diene.

which dimerizes to a cyclic template and is finally oxidized to PA[41–44].

4. Conclusion

Stoichiometric HAp and non-stoichiometric Co-HAp were successfully synthesized. Blank reactions using only HAp and Co-HAp resulted in conversions of the feed up to about 10 %, which indicate that the support itself has some activity. Total catalytic activity obtained was the resultant of the activity of the active component, the support and the active component and support interactions. Hydroxyapatite proved to be an efficient support for VPO in this study. Change in the morphology of the materials was negligible, even though the catalysts were subjected to temperatures up to 440 °C for a period of 160 hours.

The phases responsible for the activity during hydrocarbon oxidation is the vanadyl pyrophosphate, ($(VO)_2P_2O_7$) phase. There are also contributions from active sites within crystalline vanadyl(V) orthophosphate and the V^V/V^{IV} dimeric species of vanadyl phosphate. From XRD, TPR and oxidation state determination, the +4 oxidation state of V in $(VO)_2P_2O_7$ was more influential in the performance of the catalysts.

Optimum yields of up to 50 % MA and 24 % PA were obtained during the activation of *n*-pentane. In addition to the formation of the anhydrides, a number of parallel reactions took place resulting in the formation of compounds such as 1,3-pentadiene, 2-cyclopenten-1-one, furfural, furaldehyde, 1,4-dioxane-2,3-diol and 2,5-hexadione.

Acknowledgements

The aAuthor thanks the University of KwaZulu-Natal and the National Research Foundation for financial assistance.

References

1 J.J. Spivey, J.A. Anderson, K.M. Dooley and M.J. Castaldi, *Catalysis*, Royal Society of Chemistry, 2009.

2 J. Védrine, The role of redox, acid-base and collective properties and of crystalline state of heterogeneous catalysts in the selective oxidation of hydrocarbons, *Top. Catal.*, 2002, **21**, 97–106.

3 N.H. Batis, H. Batis, A. Ghorbel, J.C. Vedrine and J.C. Volta, Synthesis and characterization of new VPO catalysis for the partial *n*-butane oxidation to maleic anhydride, *J. Catal.*, 1991, **128**, 248–263.

4 H. Berndt, K. Buker, A. Martin, A. Bruckner and B. Lucke, Redox interaction of ammonia with $(VO_2)P_2O_7$, *J. Chem. Soc., Faraday Trans.*, 1995, **91**: 725–731.

5 V.A. Zazhigalov, J. Haber, J. Stoch and E.V. Cheburakova, The mechanism of *n*-pentane partial oxidation on VPO and VPBiO catalysts, *Catal. Commun*., 2001, **2**, 375–378.

6 D. Wang, H.H. Kung and M.A. Barteau, Identification of vanadium species involved in sequential redox operation of VPO catalysts, *Appl. Catal. A*., 2000, **201,** 203–213.

7 Y. Wang, X. Wang, Z. Su, Q. Guo, Q. Tang, Q. Zhang and H. Wan, SBA-15 supported iron phosphate catalyst for partial oxidation of methane to formaldehyde, *Catal. Today*, 2004, **93–95**, 155–161.

8 W. Nie, Z. Wang, W. Ji, Y. Chen and C.T. Au, Comparative studies on the VPO specimen supported on mesoporous Al-containing MCM-41 and large pore silica, *Appl. Catal. A*, 2003, **244**, 265–272.

9 S.B. Rasmussen, E. Mikolajska, M. Daturi and M.A. Bañares, Structural characteristics of an amorphous VPO monolayer on alumina for propane ammoxidation, *Catal. Today*, 2012, **192**, 96–103.

10 P.M. Michalakos, K. Birkeland and H.H. Kung, Selective oxidation of pentane over Al_2O_3- and SiO_2-supported vanadia catalysts, *J. Catal.*, 1996, **158**, 349–353.

11 F. Klose, T. Wolff, H. Lorenz, A. Seidel-Morgenstern, Y. Suchorski, M. Piórkowska and H. Weiss, Active species on γ-alumina-supported vanadia catalysts: nature and reducibility, *J. Catal.*, 2007, **247**, 176–193.

12 M.M. Bhasin, J.H. McCain, B.V. Vora, T. Imai and P.R. Pujadó, Dehydrogenation and oxydehydrogenation of paraffins to olefins, *Appl. Catal. A*., 2001, **221,** 397–419.

13 R. Subramanian, G.J. Panuccio, J.J. Krummenacher, I.C. Lee and L.D. Schmidt, Catalytic partial oxidation of higher hydrocarbons: reactivities and selectivities of mixtures, *Chem. Eng. Sci*., 2004, **59**, 5501–5507.

14 S. Sugiyama, T. Miyamoto, H. Hayashi and J.B. Moffat, Effects of non-stoichiometry of calcium and strontium hydroxyapatites on the oxidation of ethane in the presence of trichloromethane, *J. Mol. Catal. A*, 1998, **135**, 199–208.

15 K. Elkabous, M. Kacimi, M. Ziyad, S. Ammar and F. Bozon-Verduraz, Cobalt-exchanged hydroxyapatite catalysts: magnetic studies, spectroscopic investigations, performance in 2-butanol and ethane oxidative dehydrogenations, *J. Catal.*, 2004, **226**, 16–24.

16 N.Y. Mostafa and P.W. Brown, Computer simulation of stoichiometric hydroxyapatite: structure and substitutions, *J. Phys. Chem. Solids*, 2007, **68**, 431–437.

17 N. Cheikhi, M. Kacimi, M. Rouimi, M. Ziyad, L.F. Liotta, G. Pantaleo and G. Deganello, Direct synthesis of methyl isobutyl ketone in gas-phase reaction over palladium-loaded hydroxyapatite, *J. Catal*., 2005, **232**, 257–267.

18 M. Khachani, M. Kacimi, A. Ensuque, J.-Y. Piquemal, C. Connan, F. Bozon-Verduraz and M. Ziyad, Iron-calcium-hydroxyapatite catalysts: iron speciation and comparative performances in butan-2-ol conversion and propane oxydative dehydrogenation, *Appl. Catal. A*., 2010, **388,** 113–123.

19 S. Sugiyama, Y. Fujii, K. Abe, H. Hayashi and J.B. Moffat, Facile formation of the partial oxidation and oxidative-coupling products from the oxidation of methane on barium hydroxyapatites with tetrachloromethane, *Energy Fuels,* 1999, **13**, 637–640.

20 S. Sugiyama, T. Shono, D. Makino, T. Moriga and H. Hayashi, Enhancement of the catalytic activities in propane oxidation and H-D exchangebility of hydroxyl groups by the incorporation with cobalt into strontium hydroxyapatite, *J. Catal*., 2003, **214**, 8–14.

21 Y. Matsumura, S. Sugiyama, H. Hayashi, N. Shigemota, K. Saitoh and J.B. Moffat, Strontium hydroxyapatites: catalytic properties in the oxidative dehydrogenation of methane to carbon oxides and hydrogen, *J. Mol. Catal*., 1994, **92**, 81–94.

22 Z. Opre, T. Mallat and A. Baiker, Epoxidation of styrene with cobalt-hydroxyapatite and oxygen in dimethylformamide: a green technology?, *J. Catal*., 2007, **245**, 482–486.

23 S. Sebti, R. Tahir, R. Nazih, A. Saber and S. Boulaajaj, Hydroxyapatite as a new solid support for the Knoevenagel reaction in heterogenous media without solvent, *Appl. Catal. A*, 2002, **228**, 155–159.

24 A. Venugopal and M.S. Scurrell, Hydroxyapatite as a novel support for gold and ruthenium catalysts: behaviour in the water gas shift reaction, *Appl. Catal. A*., 2003, **245**, 137–147.

25 S. Sugiyama, T. Minami, H. Hayashi, M. Tanaka, N. Shigemoto and J.B. Moffat, Enhancement of the selectivity to carbon monoxide with feedstream doping by tetrachloromethane in the oxidation of methane on stoichiometric calcium hydroxyapatite, *J. Chem. Soc., Faraday Trans*., 1996, **92**, 293–299.

26 S. Singh and S.B. Jonnalagadda, Selective oxidation of *n*-pentane over V_2O_5 supported on hydroxyapatite, *Catal. Lett*., 2008, **126**, 200–206.

27 V.D.B.C. Dasireddy, S. Singh and H.B. Friedrich, Oxidative dehydrogenation of *n*-octane using vanadium pentoxide-supported hydroxyapatite catalysts, *Appl. Catal. A*., 2012, **58**, 421 422.

28 M. Campanati, G. Fornasari and A. Vaccari, Fundamentals in the preparation of heterogenous catalysts, *Catal. Today*, 2001, **77**, 299–314.

29 R.A. Sheldon and H. van Bekkum, *Fine Chemicals through Heterogeneous Catalysis*, Weinheim, Wiley, 2008.

30 K. Sing, The use of nitrogen adsorption for the characterization of porous materials, *Colloids and Surfaces A*: *Physicochem*. *Eng*. *Aspects*, 2001, **187 188**, 3–9.

31 P. Parhi, A. Ramanan and A.R. Ray, Synthesis of nano-sized alkaline-earth hydroxyapatites through microwave assisted metathesis route, *Mater. Lett*., 2006, **60**, 218–221.

32 V.V. Guliants, J.B. Benziger, S. Sundaresan, N. Yao and I.E. Wachs, Evolution of the active surface of the vanadyl pyrophosphate catalysts, *Catal. Lett*., 1995, **32**, 379–386.

33 K. Elkabous, M. Kacimi, M. Ziyad, S. Ammar, A. Ensuque, J.-Y. Piquemal and F. Bozon-Verduraz, Cobalt speciation in cobalt oxide-apatite materials: structure-properties relationship in catalytic oxidative dehydrogenation of ethane and butan-2-ol conversion, *J. Mater. Chem*., 2006, **16**, 2453–2463.

34 V.D.B.C. Dasireddy, S. Singh and H.B. Friedrich, Activation of *n*-

octane using vanadium oxide supported on alkaline earth hydroxyapatites, *Appl. Catal. A*., 2013, **456**,105–117.

35 L.M. Cornaglia, C.A. Sánchez and E.A. Lombardo, Chemistry of vanadium-phosphorus oxide catalyst preparation, *Appl. Catal. A*., 1993, **95**, 117–130.

36 F. Cavani and F. Trifirò, The characterization of the surface properties of VPO based catalysts by probe molecules, *Appl. Catal. A*, 1997, **157**, 195–221.

37 B.T. Pierini and E.A. Lombardo, Structure and properties of Cr promoted VPO catalysts, *Mater. Chem. Phys.*, 2005, **92**, 197–204.

38 X.-K. Li, W.-J. Ji, J. Zhao, Z.-B. Zhang and C.-T. Au, *n*-Butane oxidation over VPO catalysts supported on SBA-15, *J. Catal.*, 2006, **238**, 232–241.

39 G. Centi, F. Cavani and F. Trifirò, *Selective Oxidation by Heterogeneous Catalysis*, Springer, London, 2001.

40 G. Bignardi, F. Cavani, C. Cortelli, T. De Lucia, F. Pierelli, F. Trifirò, G. Mazzoni, C. Fumagalli and T. Monti, Influence of the oxidation state of vanadium for the oxidation of *n*-pentane to maleic and phthalic anhydrides, *J. Mol. Catal. A*, 2006, **244**, 244–251.

41 F. Cavani and F. Trifirò, Selective oxidation of light alkanes: interaction between the catalyst and the gas phase on different classes of catalytic materials, *Catal. Today*, 1999, **51**, 561–580.

42 G. Centi, J. Lopez-Nieto, D. Pinelli and F. Trifirò, Synthesis of phthalic and maleic anhydrides from *n*-pentane. 1. Kinetic analysis of the reaction network, *Ind. Eng. Chem. Res.*, 1989, **28**, 400–406.

43 G. Centi and F. Trifirò, Surface kinetics of adsorbed intermediates: selective oxidation of C_4-C_5 alkanes, *Chem. Eng. Sc.*, 1990, **45**, 2589–2596.

44 S. Albonetti, F. Cavani, F. Trifirò, P. Venturoli, G. Calestani, M. López Granados and J.L.G. Fierro, A comparison of the reactivity of "nonequilibrated" and "equilibrated" VPO catalysts: structural evolution, surface characterization and reactivity in the selective oxidation of *n*-butane and *n*-pentane, *J. Catal.*, 1996, **160**, 52–64.